# AC Magnetic Field Sensing Using Continuous-Wave Optically Detected Magnetic Resonance of Nitrogen Vacancy Centers in Diamond

AUTHOR(S):

Saijo, Soya; Matsuzaki, Yuichiro; Saito, Shiro; Yamaguchi, Tatsuma; Hanano, Ikuya; Watanabe, Hideyuki; Mizuochi, Norikazu; Ishi-Hayase, Junko

CITATION:

Saijo, Soya ...[et al]. AC Magnetic Field Sensing Using Continuous-Wave Optically Detected Magnetic Resonance of Nitrogen Vacancy Centers in Diamond. Applied Physics Letters 2018, 113(8): 082405.

ISSUE DATE:

2018-08-20

URL:

http://hdl.handle.net/2433/279886

APPLIED PHYSICS LETTERS **113**, 082405 (2018)

# AC magnetic field sensing using continuous-wave optically detected magnetic resonance of nitrogen-vacancy centers in diamond

Soya Saijo,[1] Yuichiro Matsuzaki,[2] Shiro Saito,[2] Tatsuma Yamaguchi,[1] Ikuya Hanano,[1] Hideyuki Watanabe,[3] Norikazu Mizuochi,[4] and Junko Ishi-Hayase[1,a)]

[1]*School of Fundamental Science and Technology, Keio University, 3-14-1 Hiyoshi, Kohoku-ku, Yokohama 223-8522, Japan*
[2]*NTT Basic Research Laboratories, NTT Corporation, 3-1 Morinosato-Wakamiya, Atsugi, Kanagawa 243-0198, Japan*
[3]*Correlated Electronics Group, Electronics and Photonics Research Institute, National Institute of Advanced Industrial Science and Technology (AIST), Tsukuba Central 5, 1-1-1 Higashi, Tsukuba, Ibaraki 305-8565, Japan*
[4]*Institute for Chemical Research, Kyoto University, Gokasho, Uji, Kyoto 611-0011, Japan*

(Received 31 January 2018; accepted 1 August 2018; published online 24 August 2018)

Nitrogen-vacancy (NV) centers in diamond can be used as highly sensitive quantum sensors for detecting magnetic fields at room temperature. Pulsed optically detected magnetic resonance (ODMR) is typically used to detect AC magnetic fields, but can only be implemented after careful calibration that involves aligning an external static magnetic field, measuring continuous-wave (CW) ODMR, determining the Rabi frequency, and setting the microwave phase. In contrast, CW-ODMR can be simply implemented by continuous application of a green CW laser and a microwave field, and can be used to detect DC or low-frequency (kHz-range) AC magnetic fields. We report a method that uses NV centers and CW-ODMR to detect high-frequency (MHz-range) AC magnetic fields. This method fully utilizes spin-1 properties of electron spins of NV centers. Unlike conventional methods, the proposed method does not require a pulse sequence; this greatly simplifies the procedure and apparatus needed for implementation. A sensitivity of 2.5 $\mu T/\sqrt{Hz}$ is found for our present experimental apparatus, the sensitivity of which is currently limited by inhomogeneous broadening and low measurement contrast of samples used and by the low collection efficiency of the optical setup, both of which could be improved in the future. Thus, this simple alternative to existing AC magnetic field sensors paves the way for the development of a practical and feasible quantum sensor. *Published by AIP Publishing.* https://doi.org/10.1063/1.5024401

Nitrogen-vacancy (NV) centers in diamond can be used to detect magnetic fields with high sensitivity and submicron spatial resolution at room temperature.[1–3] There are a number of ways in which NV centers can be employed in practice as magnetic field sensors, including, among others, vector magnetic field sensing via confocal microscopy,[4,5] rapid imaging using charge coupled device (CCD) arrays,[6–10] and atomic force microscopy, which provides nanoscale imaging using a nanodiamond or a diamond nanopillar tip.[11–15]

To implement magnetic field sensing with NV centers in diamond, either a pulsed or a continuous-wave (CW) optically detected magnetic resonance (ODMR) technique may be used. The pulsed ODMR technique has been applied to detect both AC and DC magnetic fields.[3,16,17] Although the pulsed technique provides better sensitivity than the CW-ODMR technique, it requires careful calibration before it can detect a magnetic field. This calibration typically involves measuring CW-ODMR, observing Rabi oscillations (to determine the Rabi frequency), controlling the microwave phase, and constructing a pulse sequence.

In contrast, the CW-ODMR technique can be used to detect DC magnetic fields or low frequency (e.g., in the kHz range) AC magnetic fields. It is more convenient than the pulsed technique, because it only requires the continuous application of microwaves and an optical laser. Although the sensitivity of CW-ODMR is currently less than that of pulsed ODMR, the simplicity of its experimental requirements has led to its widespread and successful magnetic field measurements.[2,7,15] In this letter, to extend the applications of CW-ODMR, we develop a method to measure high-frequency AC magnetic fields using CW-ODMR of NV centers in diamond. The CW-ODMR method has already been used to measure AC magnetic fields in the kHz frequency range; in this application, the two-level nature of NV centers is exploited.[18–20] In contrast, in the present work, we use the spin-1 properties of NV centers to measure AC magnetic fields with MHz frequencies. There are three energy eigenstates in the ground-state manifold of NV centers, all of which are used for magnetic field sensing. The lowest-energy eigenstate $|0\rangle$ is about 2.87 GHz below the two higher-energy eigenstates, which themselves have an energy difference of the order of MHz. The idea behind the proposed method is to use this MHz transition frequency to detect AC magnetic fields while the lowest-energy eigenstate is continuously excited by microwave radiation.

Note that the CW-ODMR technique is compatible with CCD-based techniques that have a slow camera frame rate. When we use a specific optical imaging setup, the magnetic field information in the diamond may be collected over a

a)Author to whom correspondence should be addressed: hayase@appi.keio.ac.jp

wide area in a single measurement,[21] and we can detect the signal by using the CCD camera. This allows the magnetic field distribution to be rapidly acquired, because, in contrast to other techniques, the magnetic field in the diamond does not need to be measured point by point.[6,7,22] The sensitivity of such a CCD camera approach depends on the imaging system to collect the photons efficiently, optimization of the delivery of the light to excite the NV centers, the sensor to record the photons, as discussed in Ref. 21. However, a potential problem with the CCD-based scheme is the slow camera operation time (from 100 Hz to 1 kHz). Since pulsed ODMR requires a pulse repetition rate exceeding a few MHz for typical AC magnetic field sensing, sophisticated techniques such as the use of optical shutters are required to improve the signal-to-noise ratio.[6,9] Conversely, because the CW-ODMR technique does not involve such fast operations, our design for an AC magnetic field sensor provides a way to adopt the CCD-based technique with a much simpler experimental setup. Furthermore, a CCD-based setup enables us to increase the measurement volume of NV centers, which results in improved sensitivity.

We start by explaining the theory behind the proposed method. The Hamiltonian of an NV center with no external magnetic field is

$$H_{\mathrm{NV}} = D\hat{S}_z^2 + E_x\left(\hat{S}_x^2 - \hat{S}_y^2\right) + E_y\left(\hat{S}_x\hat{S}_y + \hat{S}_y\hat{S}_x\right), \quad (1)$$

where $\hat{S}$ is a spin-1 operator for electron spin, $D$ is the zero-field splitting, and $E_x$ and $E_y$ are the strains in the $x$ and $y$ directions, respectively. Without loss of generality, we set $E_y = 0$ by defining the $x$ axis to pass through the NV center in the direction of the strain. Throughout this letter, we set $\hbar = 1$. The ground state is $|0\rangle$, and the two higher-energy eigenstates are defined as $|D\rangle = (|1\rangle - |-1\rangle)/\sqrt{2}$ and $|B\rangle = (|1\rangle + |-1\rangle)/\sqrt{2}$, with eigenenergies $D - E_x$ and $D + E_x$, respectively (see Fig. 1). With zero external magnetic field, two dips appear around 2.87 GHz in the CW-ODMR spectrum obtained by measuring spin-dependent photoluminescence under continuous application of a microwave field and optical laser irradiation. This indicates externally driven transitions from the ground state $|0\rangle$ to higher-energy eigenstates such as $|B\rangle$ or $|D\rangle$.[23–25]

We consider the dynamics of NV centers when both the microwave field and the target AC magnetic field are present. With these external fields, the Hamiltonian takes the form $H = H_{\mathrm{NV}} + H_{\mathrm{ex}}$, where $H_{\mathrm{ex}}$ is given by

$$H_{\mathrm{ex}} = \sum_{j=x,y,z} \gamma_e B_{\mathrm{mw}}^{(j)} \hat{S}_j \cos(\omega_{\mathrm{mw}} t) + \gamma_e B_{\mathrm{AC}}^{(j)} \hat{S}_j \cos(\omega_{\mathrm{AC}} t), \quad (2)$$

where $\gamma_e$ is the gyromagnetic ratio of the electron spin, $B_{\mathrm{mw}}$ (respectively, $B_{\mathrm{AC}}$) is the microwave field (respectively, target AC magnetic field) amplitude, and $\omega_{\mathrm{mw}}$ (respectively, $\omega_{\mathrm{AC}}$) is the frequency of the driving microwave field (respectively, target AC magnetic field). We assume that $\omega_{\mathrm{mw}}$ is of the order of GHz, whereas $\omega_{\mathrm{AC}}$ is of the order of MHz. In a rotating frame defined by $U$, the effective Hamiltonian becomes $H' = UHU^\dagger - iU(\mathrm{d}/\mathrm{d}t)U^\dagger$. By considering $U = e^{i\omega_{\mathrm{mw}} t\hat{S}_z^2}$ and using the rotating-wave approximation (RWA), we obtain the Hamiltonian

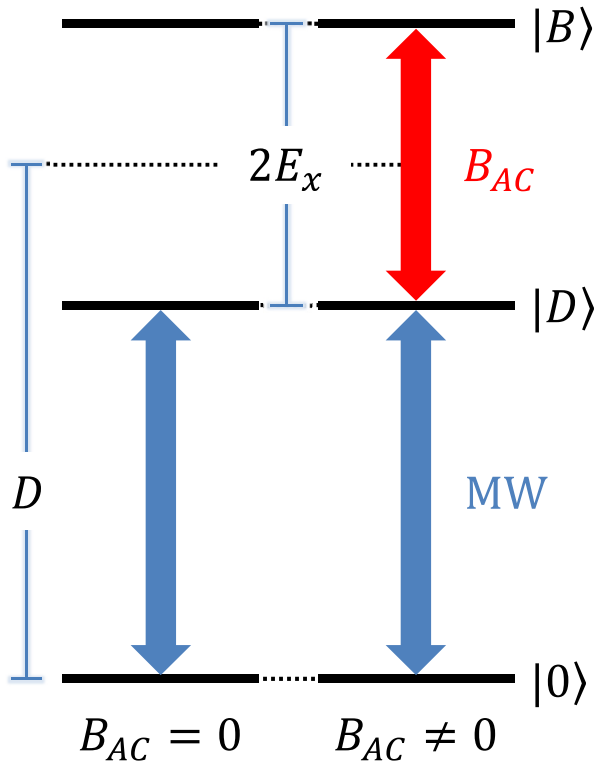


FIG. 1. Energy level diagram of an NV center in diamond. To drive these states, we apply both a GHz-frequency microwave field and a MHz-frequency AC magnetic field.

$$\begin{aligned} H \simeq\ & (D - \omega_{\mathrm{mw}})\hat{S}_z^2 + E_x\left(\hat{S}_x^2 - \hat{S}_y^2\right) \\ & + \frac{1}{2}\gamma_e B_{\mathrm{mw}}^{(x)}\hat{S}_x + \frac{1}{2}\gamma_e B_{\mathrm{mw}}^{(y)}\hat{S}_y + \gamma_e B_{\mathrm{AC}}^{(z)}\hat{S}_z\cos(\omega_{\mathrm{AC}} t), \quad (3) \\ =\ & (D + E_x - \omega_{\mathrm{mw}})|B\rangle\langle B| + (D - E_x - \omega_{\mathrm{mw}})|D\rangle\langle D| \\ & + \frac{1}{2}\gamma_e B_{\mathrm{mw}}^{(x)}(|B\rangle\langle 0| + |0\rangle\langle B|) - i\frac{1}{2}\gamma_e B_{\mathrm{mw}}^{(y)}(|D\rangle\langle 0| - |0\rangle\langle D|) \\ & + \gamma_e B_{\mathrm{AC}}^{(z)}(|B\rangle\langle D| + |D\rangle\langle B|)\cos(\omega_{\mathrm{AC}} t). \quad (4) \end{aligned}$$

In a different rotating frame defined by $U' = e^{i\frac{1}{2}\omega_{\mathrm{AC}}(\hat{S}_x^2 - \hat{S}_y^2)}$, we obtain the Hamiltonian

$$\begin{aligned} H =\ & \left(D + E_x - \omega_{\mathrm{mw}} - \frac{1}{2}\omega_{\mathrm{AC}}\right)|B\rangle\langle B| \\ & + \left(D - E_x - \omega_{\mathrm{mw}} + \frac{1}{2}\omega_{\mathrm{AC}}\right)|D\rangle\langle D| \\ & + \frac{1}{2}\gamma_e B_{\mathrm{mw}}^{(x)}\left(e^{i\frac{1}{2}\omega_{\mathrm{AC}} t}|B\rangle\langle 0| + e^{-i\frac{1}{2}\omega_{\mathrm{AC}} t}|0\rangle\langle B|\right) \\ & - i\frac{1}{2}\gamma_e B_{\mathrm{mw}}^{(y)}\left(e^{-i\frac{1}{2}\omega_{\mathrm{AC}} t}|D\rangle\langle 0| - e^{i\frac{1}{2}\omega_{\mathrm{AC}} t}|0\rangle\langle D|\right) \\ & + \frac{1}{2}\gamma_e B_{\mathrm{AC}}^{(z)}(|B\rangle\langle D| + |D\rangle\langle B|), \quad (5) \end{aligned}$$

where we have again used the RWA.

Importantly, an AC magnetic field in the $z$ direction [the fifth term in the Hamiltonian (5)] induces the transition between $|B\rangle$ and $|D\rangle$ when the frequency of the AC magnetic field is in resonance with the energy difference between $|B\rangle$ and $|D\rangle$. Without the AC magnetic field, we can only induce transitions between the ground state $|0\rangle$ and the bright

(respectively, dark) state $|B\rangle$ (respectively, $|D\rangle$) via microwave radiation of frequency $\omega_{\rm mw} \simeq D + E_x$ (respectively, $\omega_{\rm mw} \simeq D - E_x$) in the conventional CW-ODMR setup. However, combining the applied AC magnetic field and the microwave field can drive transitions from the ground state to the bright and dark states. Thus, the results of CW-ODMR with an applied AC magnetic field should differ from those of CW-ODMR in the absence of an AC magnetic field.

We now quantify the change in the CW-ODMR signal attributable to the AC magnetic fields. For simplicity, we focus on the transition between $|B\rangle$ and $|D\rangle$ induced by applying an AC magnetic field of frequency $\omega_{\rm AC} = 2E_x$. We assume a weak amplitude for the AC magnetic field so that we can use time-dependent perturbation theory. In the interaction picture, we obtain

$$\begin{aligned} H_I = &\frac{1}{2\sqrt{2}}\gamma_e B_{\rm mw}^{(x)}\left[\exp\left\{i\left(D+E_x+\frac{1}{2}\gamma_e B_{\rm AC}^{(z)}-\omega_{\rm mw}\right)t\right\}|1\rangle\langle 0| \right. \\ &\left. +\exp\left\{i\left(D+E_x-\frac{1}{2}\gamma_e B_{\rm AC}^{(z)}-\omega_{\rm mw}\right)t\right\}|-1\rangle\langle 0|+{\rm hc}\right] \\ &-i\frac{1}{2\sqrt{2}}\gamma_e B_{\rm mw}^{(y)}\left[\exp\left\{i\left(D-E_x+\frac{1}{2}\gamma_e B_{\rm AC}^{(z)}-\omega_{\rm mw}\right)t\right\}|1\rangle\langle 0| \right. \\ &\left. -\exp\left\{i\left(D-E_x-\frac{1}{2}\gamma_e B_{\rm AC}^{(z)}-\omega_{\rm mw}\right)t\right\}|-1\rangle\langle 0|+{\rm hc}\right]. \end{aligned} \tag{6}$$

By using Fermi's golden rule, we can show that for the transition from the ground state to the higher-energy eigenstates, we must have $\omega_{\rm mw} \simeq D \pm E_x \pm \gamma_e B_{\rm AC}^{(z)}/2$ (Fig. 1). Thus, applying an external AC magnetic field changes the dip structure of the CW-ODMR spectrum. Actually, as we will explain below, we experimentally observe such a change in the CW-ODMR (Fig. 2).

We now describe the details of the diamond sample used in our experiment. We use an ensemble of NV centers in a 100 nm-thick diamond film on a (001) electronic-grade substrate. The isotopically purified $^{12}$C diamond film ($[^{12}{\rm C}] = 99.999\%$) was grown using nitrogen-doped microwave plasma-assisted chemical vapor deposition. To both increase the NV center density and improve the coherence time,[26] the sample was irradiated with 15 keV $He^+$ ions at ion doses of $10^{12}\,{\rm cm}^{-3}$, followed by annealing for 24 h in vacuum at 800 °C. The densities of NV and N were estimated to be of the order of $10^{15}$ and $10^{17}\,{\rm cm}^{-3}$, respectively.[27] In our experiment, we use a diamond sample with asymmetric orientation in the four crystallographic axes, where the orientation of about 40% of the NV centers is aligned to one axis.

We now explain the experimental setup for sensing an AC magnetic field using CW-ODMR. We use a home-built system for confocal laser scanning microscopy with a spatial resolution of 400 nm. The diamond sample is positioned above the antenna[28] used to emit the microwaves. A 30 $\mu$m-diameter copper wire is placed in contact with the sample surface to apply the target AC magnetic field, which is detected by measuring the difference in the CW-ODMR spectrum. We use a single-photon resolving detector to measure the photons from the NV centers. No external DC magnetic field is applied in any of the experiments.

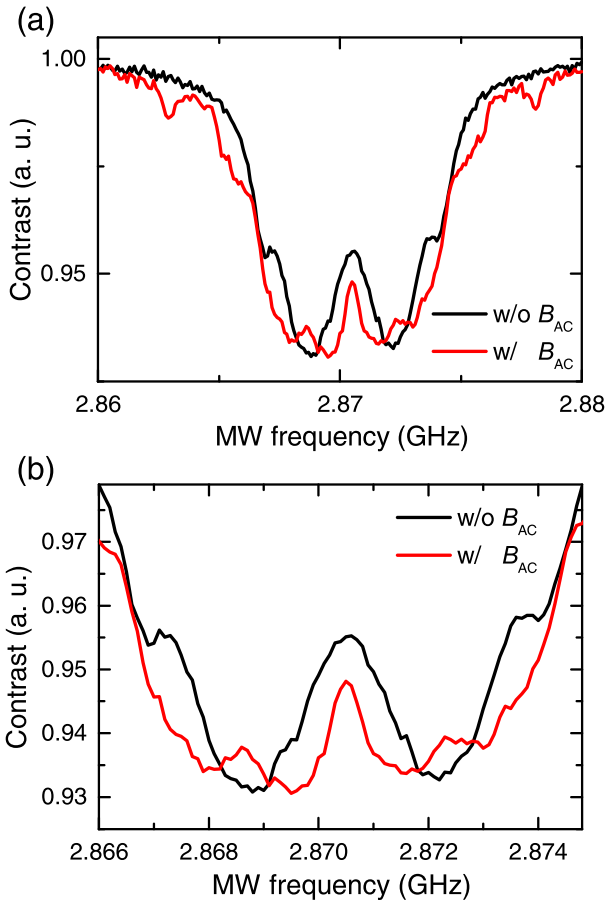


FIG. 2. (a) ODMR with and without an AC magnetic field ($B_{\rm AC}\cos 2\pi f_{\rm AC}$) for $B_{\rm AC} = 7.7\,\mu$T and $f_{\rm AC} = 4$ MHz. Here, no DC magnetic field is applied. The application of an AC magnetic field changes the ODMR spectrum. (b) The enlarged view of (a).

First, we measure the conventional CW-ODMR spectrum with no external AC magnetic field (see Fig. 2). The resonance frequency is split by approximately 4 MHz because of the local magnetic field and strain from impurities in the diamond.[24,25] This splitting leads to the energy difference between $|B\rangle$ and $|D\rangle$. Thus, CW-ODMR is performed by applying an AC magnetic field of frequency $f_{\rm AC} = \omega_{\rm AC}/2\pi = 4$ MHz and magnetic field amplitude $B_{\rm AC} = 7.7\,\mu$T to induce transitions between $|B\rangle$ and $|D\rangle$. The result in Fig. 2 shows the difference in the spectrum due to the external AC magnetic field, as our theoretical model predicts. This result clearly demonstrates the detection of an external AC magnetic field by CW-ODMR.

Since we use the resonance between $|B\rangle$ and $|D\rangle$, the detectable frequency range of AC magnetic fields is determined by the splitting between $|B\rangle$ and $|D\rangle$. As noted in Eq. (5), this splitting can be changed by applying an electric field. This fact provides a way to determine which frequencies of the AC magnetic field will be detected. Although the use of electric fields to tune the AC frequency requires additional complexity in the device, there have been some experimental demonstrations of the application of electric fields to NV centers, and so this approach is feasible using current technology.[29] Straightforward calculations show that the detectable frequencies range from hundreds of kHz to hundreds of MHz. The lower limit is determined by the resonance linewidth of the ODMR spectrum, with 200 kHz being

the current minimum reported linewidth,[26] which gives us the frequency resolution of our sensing scheme. The upper limit is determined by the breakdown field in diamond. The splitting due to the Stark effect is given as $2RE_x$. Since the Stark shift constant $R = 17\,\mathrm{Hz}\cdot\mathrm{cm/V}$,[30] and the breakdown electric field of diamond $E = 10\,\mathrm{MV/m}$,[31] the maximum splitting width is estimated to be 340 MHz, which shows the dynamic range of our approach. Thus, the proposed method may provide a simpler way to detect high-frequency (above 100 MHz) AC magnetic fields compared with the conventional method using pulsed ODMR. With the latter method, although it is technically possible to detect high-frequency AC magnetic fields by narrowing the pulse interval, it is not easy in practice because of the need to increase the Rabi frequency of the NV centers and the cost of the high-speed control device that is required.

Next, we measure the dependence of ODMR on the amplitude of the AC magnetic field. The ODMR spectrum for various AC magnetic field amplitudes is shown in Fig. 3, where we set $f_{\mathrm{AC}} = 4$ MHz. In the presence of an AC magnetic field, there are four resonances, compared with just two in the absence of such a field, and the splitting between lines becomes larger with increasing amplitude of the field. This is consistent with the formula that we derived for the resonance: $\omega_{\mathrm{mw}} \simeq D \pm E_x \pm \gamma_e B_{\mathrm{AC}}^{(z)}/2$. Therefore, the amplitude of an AC magnetic field can be estimated by measuring the resonance frequency or the ODMR signal intensity at a fixed microwave frequency.

In Fig. 4(a), we plot the ODMR signal against the amplitude of the AC magnetic field, at a microwave frequency $f_{\mathrm{mw}} = \omega_{\mathrm{mw}}/2\pi = 2.86887$ GHz, which is one of the two resonance frequencies obtained in the absence of an external AC magnetic field. The signal depends quadratically on the amplitude. Such a quadratic dependence can be quantitatively understood as follows. We represent the two resonances around $D - E_x$ as the sum of two Lorentzian functions: $F(B) = \sum_{j=\pm1}[\{f_{\mathrm{mw}} - (D + j\gamma_e B_{\mathrm{AC}}^{(z)}/2 - E_x)\}^2 + \gamma^2]^{-1}$, where $\gamma$ is the linewidth. We obtain $\mathrm{d}F(B)/\mathrm{d}B \propto B$ for small $B$, which shows the quadratic dependence.

To estimate the magnetic sensitivity $\delta B_{AC}$ from the experimental results, we must determine the signal fluctuation $\delta S$, where $S$ corresponds to the photoluminescence in ODMR.[3] As shown in Fig. 4(b), the fluctuation decreases with a square-root dependence $\sqrt{T}$, where $T$ is the measurement time. From these experimental results, we estimate

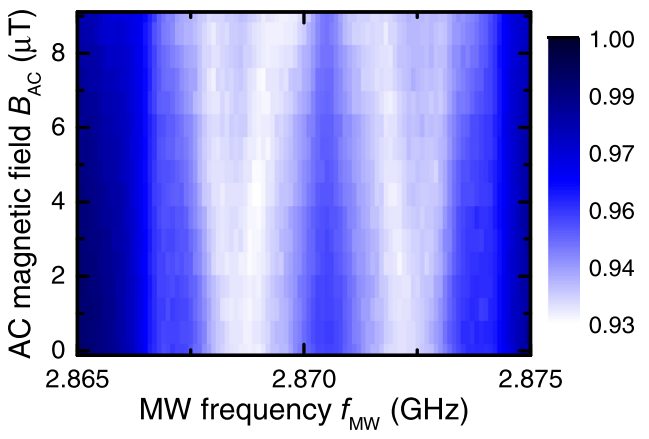


FIG. 3. ODMR spectrum with an applied AC magnetic field. Four resonances are observed in the presence of an AC magnetic field.

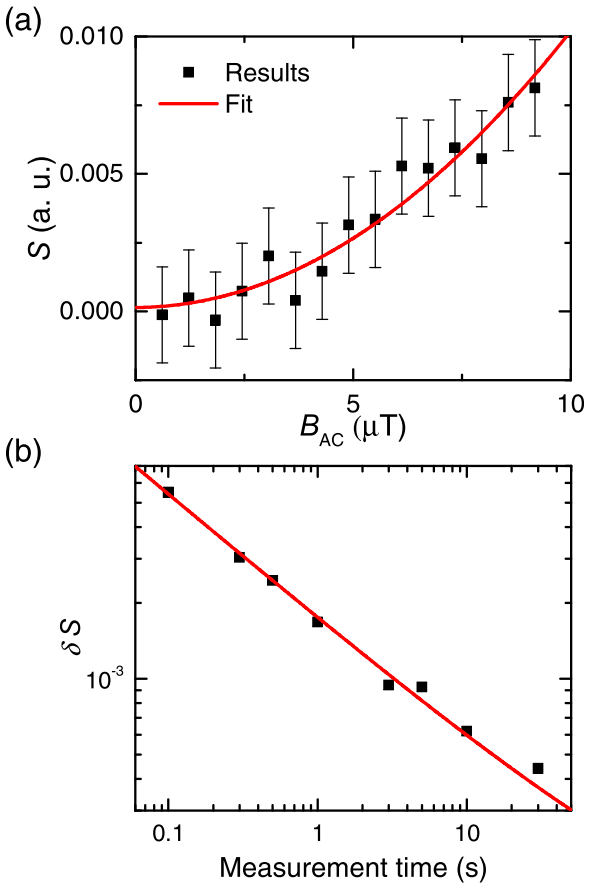


FIG. 4. Measured signal and standard deviation of the ODMR signal. (a) ODMR signal plotted against the amplitude of the AC magnetic field. The data are fitted to the function $S - S_0 = a(B_{\mathrm{AC}})^2$, where $a$ is a fitting parameter and $S_0$ is the offset. The fit shows that the signal is quadratic in the amplitude of the AC magnetic field. (b) Standard deviation $\delta S$ of the ODMR signal as a function of measurement time.

the sensitivity for detecting AC magnetic fields with a measurement time of 1 s to be $2.5\,\mu\mathrm{T}/\sqrt{\mathrm{Hz}}$. The low contrast (<10%) of our device is one of the limitations on its sensitivity. Also, inhomogeneous broadening of the NV centers induces a large width in the ODMR, which also decreases the sensitivity. Note that the sensitivity could be improved by using a NV center in diamond with a narrow linewidth[26] and with an almost perfect preferential orientation of the axis[32–34] and a high density of NV centers.[26,34,35] In fact, there is a report of a diamond with a contrast of 27%, an NV density of more than $10^{16}\,\mathrm{cm}^{-3}$, and nearly perfectly aligned NV centers along one crystallographic axis.[34] Using these parameters, we estimate the expected sensitivity of the proposed method to be $50\,\mathrm{nT}/\sqrt{\mathrm{Hz}}$ with submicron spatial resolution maintained. The sensitivity could be further improved by increasing the detection volume. Although a diamond sample with a perfect single orientation of the NV centers among the crystal defects has yet to be obtained, much effort has been devoted to realizing such perfect alignment and preferential orientation. In fact, samples in which more than 99% of NV centers are aligned in one direction have been produced,[32–34] and thus our predicted sensitivity should be within the reach of near-future technology. Finally, we discuss possible applications of our scheme. First, our AC field detection would be useful to read out the state of a

superconducting flux qubit (FQ).[36] The NV centers can be coupled with the FQ via the magnetic fields from the persistent current of the FQ.[37–40] In particular, if we drive the FQ by Rabi oscillations, it will induce AC magnetic fields. Suppose that the persistent current is around 1 $\mu$A[37] and the energy relaxation time is around 100 $\mu$s.[41] Then, AC magnetic field measurements with a sensitivity of tens of nanotesla and a spatial resolution of hundreds of nanometers can read out the state of the flux qubit within the coherence time. A large applied magnetic field is incompatible with superconductivity, and so such a readout should be done with zero or near-zero applied magnetic field, which is possible with our scheme. Another possible application is the wide-field imaging of current flow in nanodevices consisting of graphene, carbon nanotubes, etc. Wide-field imaging provides a powerful tool to measure the spatial distribution of the current flow in such nanodevices, which provides important information about their performance and the physics involved. Moreover, wide-field imaging has a significantly decreased total measurement time compared with scanning confocal microscopy. Our technique for AC magnetic field sensing using CW-ODMR is particularly compatible with wide-field imaging using CCD cameras with slow response time.

In conclusion, we have proposed and demonstrated a method to detect high-frequency AC magnetic fields that uses CW-ODMR by exploiting NV centers in diamond. By simply applying a continuous microwave field and optical laser irradiation, the method provides a sensitivity of $2.5\,\mu\mathrm{T}/\sqrt{\mathrm{Hz}}$ at room temperature. The experimental setup is very simple because it does not require a pulse sequence. These results pave the way to realizing a practical and feasible AC magnetic field sensor.

We thank H. Toida and K. Kakuyanagi for helpful discussions. This work was supported by JSPS KAKENHI (Grant No. 15K17732) and MEXT KAKENHI (Grant Nos. 15H05868, 15H05870, 15H03996, 26220602, and 26249108). This work was also supported by the Advanced Photon Science Alliance (APSA), JSPS Core-to-Core Program FY2013 Projects No. 2, and Spin-NRJ.

[1]T. Wolf, P. Neumann, K. Nakamura, H. Sumiya, T. Ohshima, J. Isoya, and J. Wrachtrup, Phys. Rev. X **5**, 041001 (2015).
[2]G. Balasubramanian, I. Y. Chan, R. Kolesov, M. Al-Hmoud, J. Tisler, C. Shin, C. Kim, A. Wojcik, P. R. Hemmer, A. Krueger, T. Hanke, A. Leitenstorfer, R. Bratschitsch, F. Jelezko, and J. Wrachtrup, Nature **455**, 648 (2008).
[3]J. M. Taylor, P. Cappellaro, L. Childress, L. Jiang, D. Budker, P. R. Hemmer, A. Yacoby, R. Walsworth, and M. D. Lukin, Nat. Phys. **4**, 810 (2008).
[4]B. J. Maertz, A. P. Wijnheijmer, G. D. Fuchs, M. E. Nowakowski, and D. D. Awschalom, Appl. Phys. Lett. **96**, 092504 (2010).
[5]R. S. Schoenfeld and W. Harneit, Phys. Rev. Lett. **106**, 030802 (2011).
[6]L. M. Pham, D. Le Sage, P. L. Stanwix, T. K. Yeung, D. Glenn, A. Trifonov, P. Cappellaro, P. R. Hemmer, M. D. Lukin, H. Park, A. Yacoby, and R. L. Walsworth, New J. Phys. **13**, 045021 (2011).
[7]D. Le Sage, K. Arai, D. R. Glenn, S. J. Devience, L. M. Pham, L. Rahn-Lee, M. D. Lukin, A. Yacoby, A. Komeili, and R. L. Walsworth, Nature **496**, 486 (2013).
[8]S. Steinert, F. Ziem, L. T. Hall, A. Zappe, M. Schweikert, N. Götz, A. Aird, G. Balasubramanian, L. Hollenberg, and J. Wrachtrup, Nat. Commun. **4**, 1607 (2013).
[9]S. J. Devience, L. M. Pham, I. Lovchinsky, A. O. Sushkov, N. Bar-Gill, C. Belthangady, F. Casola, M. Corbett, H. Zhang, M. Lukin, H. Park, A. Yacoby, and R. L. Walsworth, Nat. Nanotechnol. **10**, 129 (2015).
[10]D. R. Glenn, K. Lee, H. Park, R. Weissleder, A. Yacoby, M. D. Lukin, H. Lee, R. L. Walsworth, and C. B. Connolly, Nat. Methods **12**, 736 (2015).
[11]P. Maletinsky, S. Hong, M. S. Grinolds, B. Hausmann, M. D. Lukin, R. L. Walsworth, M. Loncar, and A. Yacoby, Nat. Nanotechnol. **7**, 320 (2012).
[12]L. Rondin, J. P. Tetienne, P. Spinicelli, C. Dal Savio, K. Karrai, G. Dantelle, A. Thiaville, S. Rohart, J. F. Roch, and V. Jacques, Appl. Phys. Lett. **100**, 153118 (2012).
[13]J.-P. Tetienne, T. Hingant, J.-V. Kim, L. H. Diez, J.-P. Adam, K. Garcia, J.-F. Roch, S. Rohart, A. Thiaville, D. Ravelosona, and V. Jacques, Science **344**, 1366 (2014).
[14]P. Appel, E. Neu, M. Ganzhorn, A. Barfuss, M. Batzer, M. Gratz, A. Tschöpe, and P. Maletinsky, Rev. Sci. Instrum. **87**, 063703 (2016).
[15]K. Chang, A. Eichler, J. Rhensius, L. Lorenzelli, and C. L. Degen, Nano Lett. **17**, 2367 (2017).
[16]C. L. Degen, Appl. Phys. Lett. **92**, 243111 (2008).
[17]J. R. Maze, P. L. Stanwix, J. S. Hodges, S. Hong, J. M. Taylor, P. Cappellaro, L. Jiang, M. V. G. Dutt, E. Togan, A. S. Zibrov, A. Yacoby, R. L. Walsworth, and M. D. Lukin, Nature **455**, 644 (2008).
[18]K. Jensen, N. Leefer, A. Jarmola, Y. Dumeige, V. M. Acosta, P. Kehayias, B. Patton, and D. Budker, Phys. Rev. Lett. **112**, 160802 (2014).
[19]S. Ahmadi, H. A. El-Ella, J. O. Hansen, A. Huck, and U. L. Andersen, Phys. Rev. Appl. **8**, 034001 (2017).
[20]T. Tashima, H. Morishita, and N. Mizuochi, preprint arXiv:1712.04615 (2017).
[21]A. M. Wojciechowski, M. Karadas, A. Huck, C. Osterkamp, S. Jankuhn, J. Meijer, F. Jelezko, and U. L. Andersen, Rev. Sci. Instrum. **89**, 031501 (2018).
[22]J.-P. Tetienne, N. Dontschuk, D. A. Broadway, A. Stacey, D. A. Simpson, and L. C. L. Hollenberg, Sci. Adv. **3**, e1602429 (2017).
[23]K. Fang, V. M. Acosta, C. Santori, Z. Huang, K. M. Itoh, H. Watanabe, S. Shikata, and R. G. Beausoleil, Phys. Rev. Lett. **110**, 130802 (2013).
[24]X. Zhu, Y. Matsuzaki, R. Amsüss, K. Kakuyanagi, T. Shimo-Oka, N. Mizuochi, K. Nemoto, K. Semba, W. J. Munro, and S. Saito, Nat. Commun. **5**, 3424 (2014).
[25]Y. Matsuzaki, H. Morishita, T. Shimooka, T. Tashima, K. Kakuyanagi, K. Semba, W. J. Munro, H. Yamaguchi, N. Mizuochi, and S. Saito, J. Phys.: Condens. Matter **28**, 275302 (2016).
[26]E. E. Kleinsasser, M. M. Stanfield, J. K. Q. Banks, Z. Zhu, W.-D. Li, V. M. Acosta, H. Watanabe, K. M. Itoh, and K.-M. C. Fu, Appl. Phys. Lett. **108**, 202401 (2016).
[27]H. Watanabe, T. Kitamura, S. Nakashima, and S. Shikata, J. Appl. Phys. **105**, 093529 (2009).
[28]K. Sasaki, E. E. Kleinsasser, Z. Zhu, W. D. Li, H. Watanabe, K. M. C. Fu, K. M. Itoh, and E. Abe, Appl. Phys. Lett. **110**, 192407 (2017).
[29]T. Iwasaki, W. Naruki, K. Tahara, T. Makino, H. Kato, M. Ogura, D. Takeuchi, S. Yamasaki, and M. Hatano, ACS Nano **11**, 1238 (2017).
[30]E. Van Oort and M. Glasbeek, Chem. Phys. Lett. **168**, 529 (1990).
[31]A. T. Collins, *Properties and Growth of Diamond* (Inspec, 1994).
[32]J. Michl, T. Teraji, S. Zaiser, I. Jakobi, G. Waldherr, F. Dolde, P. Neumann, M. W. Doherty, N. B. Manson, J. Isoya, and J. Wrachtrup, Appl. Phys. Lett. **104**, 102407 (2014).
[33]T. Fukui, Y. null, T. Miyazaki, Y. Miyamoto, H. Kato, T. Matsumoto, T. Makino, S. Yamasaki, R. Morimoto, N. Tokuda, M. Hatano, Y. Sakagawa, H. Morishita, T. Tashima, S. Miwa, Y. Suzuki, and N. Mizuochi, Appl. Phys. Express **7**, 055201 (2014).
[34]H. Ozawa, K. Tahara, H. Ishiwata, M. Hatano, and T. Iwasaki, Appl. Phys. Express **10**, 045501 (2017).
[35]V. M. Acosta, E. Bauch, M. P. Ledbetter, C. Santori, K.-M. C. Fu, P. E. Barclay, R. G. Beausoleil, H. Linget, J. F. Roch, F. Treussart, S. Chemerisov, W. Gawlik, and D. Budker, Phys. Rev. B **80**, 115202 (2009).
[36]J. Clarke and F. K. Wilhelm, Nature **453**, 1031 (2008).
[37]J. Twamley and S. D. Barrett, Phys. Rev. B **81**, 241202 (2010).
[38]D. Marcos, M. Wubs, J. Taylor, R. Aguado, M. D. Lukin, and A. S. Sørensen, Phys. Rev. Lett. **105**, 210501 (2010).
[39]Y. Matsuzaki, X. Zhu, K. Kakuyanagi, H. Toida, T. Shimooka, N. Mizuochi, K. Nemoto, K. Semba, W. Munro, H. Yamaguchi, and S. Saito, Phys. Rev. A **91**, 042329 (2015).
[40]Y. Matsuzaki, X. Zhu, K. Kakuyanagi, H. Toida, T. Shimo-Oka, N. Mizuochi, K. Nemoto, K. Semba, W. J. Munro, H. Yamaguchi, and S. Saito, Phys. Rev. Lett. **114**, 120501 (2015).
[41]F. Yan, S. Gustavsson, A. Kamal, J. Birenbaum, A. P. Sears, D. Hover, T. J. Gudmundsen, D. Rosenberg, G. Samach, S. Weber, J. L. Yoder, T. P. Orlando, J. Clarke, A. J. Kerman, and W. D. Oliver, Nat. Commun. **7**, 12964 (2016).